AIAA JOURNAL
Vol. 32, No. 3, March 1994

# Nonreflective Boundary Conditions for High-Order Methods

H. Atkins*
*NASA Langley Research Center, Hampton, Virginia 23681*
and
Jay Casper†
*ViGYAN, Inc., Hampton, Virginia 23666*

**A different approach to nonreflective boundary conditions for the Euler equations is presented. This work is motivated by a need for inflow and outflow boundary conditions that do not limit the useful accuracy of high-order accurate methods. The primary interest is in the propagation and convection of continuous acoustic and convective waves. This new approach employs the exact solution to finite waves to relate interior values and ambient conditions to boundary values. The method is first presented in one dimension and then generalized to multidimensions. Grid refinement studies are used to demonstrate high-order convergence for both one-dimensional and two-dimensional flows.**

## Introduction

NONREFLECTIVE boundary treatments can be broadly grouped into two categories: buffer zone methods and characteristic-based methods. In the buffer zone method, the physical domain of interest is supplemented by a zone in which the governing equations are modified. The modification may take on any number of forms, but it usually involves decreasing the streamwise dissipation and increasing either the convection speed[1] or the crossflow dissipation.[2] Both modifications are applicable only to multidimensional viscous flowfields because significant dissipation is assumed to exist in the crossflow direction. In both cases, the modification produces nonphysical results within the buffer zone and relies on the convective nature of the modified equations to carry the errors out of the domain. Although the approach has been successfully applied on boundaries where the fluid exits the domain, such an approach is clearly not applicable on boundaries where the fluid enters the domain.

The characteristic-based methods are applicable to both inflow and outflow boundaries that are dominated by wave propagation. Naturally, this approach is most popular in fields where acoustics are of interest. The philosophy of this approach is that waves entering the domain can be identified and suppressed or eliminated at the equation level.

Although there are many variations on this theme,[3–5] they all have the same basic limitations. Formal justification[3] of this approach relies on the existence of Riemann invariants. This property guarantees that each wave can be completely decoupled from all other possible waves. However, a full and unique set of Riemann invariants does not exist, even in one dimension, for general solutions to the Euler equations, except under the assumption of isolated simple waves.[6] Thus, in practice, inbound waves are identified and approximately eliminated by the use of a local linearization of the Euler equations.

Additionally, most characteristic-based methods are inherently one dimensional and produce considerable error when oblique waves attempt to pass out of the domain; however, the recent work of Giles[7] and Saxer and Giles,[8] which approximately accounts for multidimensional effects, has had some success.

A side effect of eliminating inbound waves is that the interior solution is decoupled from the ambient conditions. Such a procedure places an extreme burden on the flow solver from a stability perspective. In particular, the numerical flow solver, combined with boundary conditions and closure relations, must possess a properly bounded energy norm to insure stability.[9] Many common flow solvers have not been analyzed in this regard.

Because the errors produced by characteristic methods are due to the linearization, the approach works perfectly well for linear problems and is usually acceptable for flows with very small perturbations or flows simulated by low-order accuracy methods.

The objective of this work is to formulate inflow and outflow boundary conditions that are nonreflective to the order of accuracy of the numerical flow solver and are independent of wave amplitude. In the present approach, the issue of nonreflectivity is viewed from a different perspective. In particular, instead of attempting to eliminate inbound waves, the present method stresses the importance of accurately treating both inbound and outbound waves and their nonlinear coupling. This approach is motivated by the following observation: if the far field is quiescent, then the only waves that can possibly reach the boundary are those waves that originated within the computational domain. Hence, any unexpected (nonphysical) inbound wave that originates at the boundary can arise only from improper treatment of an outbound wave. In practice, however, numerical disturbances that reach the boundary consist of exact outbound waves plus truncation error. Thus, even an exact treatment of a numerically generated outbound wave would result in a reflection because the truncation error could be interpreted as an inbound wave. Because it is unreasonable to expect any boundary condition to remove all truncation error, the approach chosen here is to accurately represent the physics of the inbound waves to insure their amplitudes are related only to the truncation error of the flow solver and not nonlinear effects of the boundary condition itself.

In addition to preserving the high-order convergence of the flow solver, the method described here recognizes that the boundary of the computational domain is usually smaller than the true domain of the physical problem and that a sufficiently complete description of the solution at the computational boundary is usually not known a priori. The present method accurately accommodates this common situation by assuming that known ambient conditions exist at some distant point exterior to the computational domain and that the computational domain is connected to the ambient conditions by finite amplitude waves. Hence, the present boundary condition is referred to as the finite wave model.

Presented as Paper 93-0152 at the AIAA 31st Aerospace Sciences Meeting, Reno, NV, Jan. 11–14, 1993; received March 23, 1993; revision received Sept. 18, 1993; accepted for publication Sept. 20, 1993. 

*Research Scientist, Computational Aerodynamics Branch, Fluid Mechanics Division. Member AIAA.

†Research Engineer, Advanced Technology Research Group, 30 Research Drive. Member AIAA.

The first part of this paper describes the finite wave model boundary condition for a one-dimensional flow, followed by extensions to multidimensional flows. Although the basic concept of the multidimensional extension is general, some of the information needed for its implementation is dependent on the type of flow under consideration. Multidimensional cases discussed here include channel flows with oblique acoustic wave patterns, supersonic flows in which the component of the flow that is normal to the boundary is subsonic, and subsonic flows in which the outer boundary is at some distance from the source of the disturbance. The finite wave model has been applied to both control-volume[10] and finite difference[11] methods; however, all of the validations presented here use a fourth-order control-volume method based on an essentially nonoscillatory (ENO) approach. A description of the implementation of the finite wave model, as well as that of the characteristic-based method to which it is compared, is given. The flow solver is not discussed here, but may be found in the cited references.

## Finite Wave Model in One Dimension

Figure 1 contains diagrams that are typically used to illustrate characteristic methods and Riemann methods. Although both represent similar physical information, their perspectives of the flow are quite different. In the characteristic approach (Fig. 1a), data paths, which are also wave paths, converge on a point in $(x, t)$ space where the solution is desired. In the Riemann approach (Fig. 1b), the wave paths diverge away from the point of interest. The finite wave model boundary condition (Fig. 1c) views the flow from the perspective of the Riemann problem. The major difference is that points **a** and **b** of Fig. 1c are not assumed to be coincident in space but instead are assumed to be separated by a finite distance, which allows compressions to exist as acoustic waves. The advantage of the Riemann perspective is that each wave is considered a simple wave, which permits the legitimate use of Riemann invariants. Because our primary interest is in acoustic simulations, all compressions will be assumed to be acoustic waves, although, strictly speaking, shocks may still exist. Thus, the finite wave model assumes that points **a** and **b** are separated by left- and right-traveling acoustic waves and a convecting entropy wave. This assumption greatly simplifies the mathematics, when compared with a true Riemann problem, because the set of equations that describes this wave structure can be solved in closed form without iteration. It should be noted that a similar physical interpretation of the flow topology was used by Osher and Chakravarthy[12] in the development of a numerical flux formula; however, the multidimensional aspect of the present approach is quite different.

The equations that govern the wave structure are readily found in any classical compressible-flow text[13]:

$$U_2 - U_1 = \frac{-2n}{\gamma - 1}(a_2 - a_1) \tag{1a}$$

$$\frac{a_2}{a_1} = \left(\frac{P_2}{P_1}\right)^{\frac{\gamma-1}{2\gamma}} \tag{1b}$$

$$U_3 = U_2 \tag{1c}$$

$$P_3 = P_2 \tag{1d}$$

$$U_4 - U_3 = \frac{2n}{\gamma - 1}(a_4 - a_3) \tag{1e}$$

$$\frac{a_4}{a_3} = \left(\frac{P_4}{P_3}\right)^{\frac{\gamma-1}{2\gamma}} \tag{1f}$$

where the subscript denotes the state, $U$ is the flow speed, $a$ is the sound speed, $P$ is the pressure, and $n$ is a sign parameter (+1 or −1) that is introduced for convenience and discussed later. Equations (1a) and (1b) describe a left-traveling acoustic wave; Eqs. (1c) and (1d) describe a convective entropy wave; and Eqs. (1e) and (1f) describe a right-traveling acoustic wave. Equations (1a–f) can be rearranged to give the properties at states 2 and 3 in terms of the properties at states 1 and 4 (or **a** and **b**):

$$a_2 = a_1 \left[ \frac{n\frac{\gamma-1}{2}(U_1 - U_4) + a_1 + a_4}{a_1 + a_4\left(\frac{P_1}{P_4}\right)^{\frac{\gamma-1}{2\gamma}}} \right] \tag{2a}$$

$$P_3 = P_2 = P_1\left(\frac{a_2}{a_1}\right)^{\frac{2\gamma}{\gamma-1}} \tag{2b}$$

$$a_3 = a_4\left(\frac{P_3}{P_4}\right)^{\frac{\gamma-1}{2\gamma}} \tag{2c}$$

$$U_3 = U_2 = U_1 - \frac{2n}{\gamma - 1}(a_2 - a_1) \tag{2d}$$

Because the finite wave model depends only on the flow at points **a** and **b** and not on solution derivatives, these points can be thought of as states in the solution space and should not be attached to any particular spatial point. As a matter of convention, let state **a** denote the ambient state and state **b** denote the boundary state as determined by the numerical flow solver. Because the relations governing left- and right-traveling waves differ only by a sign, information about the direction of the path from point **a** to **b**

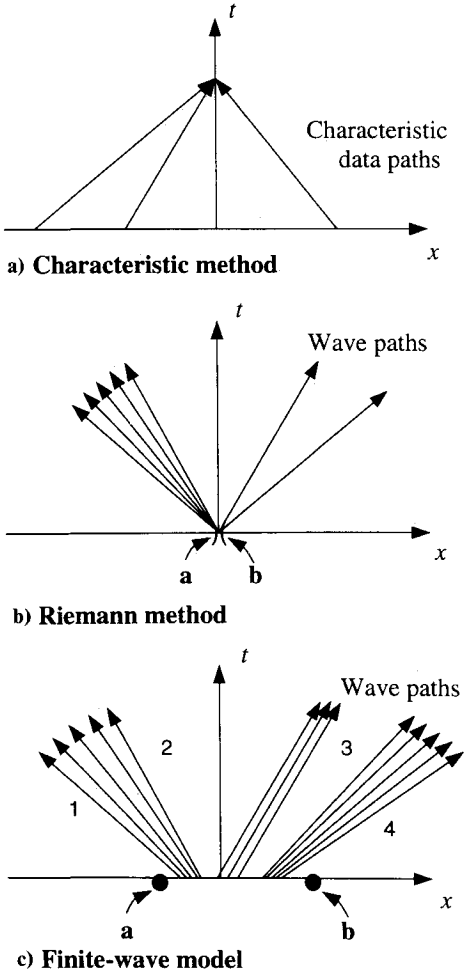


**Fig. 1 Schematic representations of wave motion.**

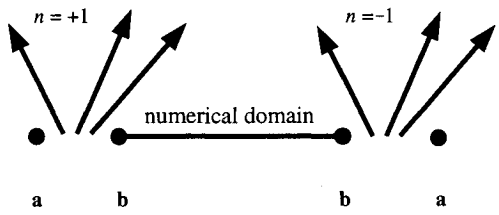


**Fig. 2 Relation between the direction of a right-traveling wave and the points a and b depends on the boundary's orientation to the domain.**

must be preserved. This is the function of the parameter $n$, which is illustrated in Fig. 2. On the left side of the domain, a right-traveling wave moves from **a** to **b** and $n = +1$; on the right side of the domain, the same wave moves from **b** to **a** and $n = -1$. Finally, because no constraints on the nature of the ambient conditions exist, the method applies equally well to cases with steady or unsteady ambient conditions. Consequently, the finite wave model not only prevents reflections of outbound waves, but it also allows inbound waves to be imposed on the flowfield when desired. *The boundary state sought is either state 2 or state 3 depending on the direction of the flow.* When the flow direction is into the domain, from **a** to **b**, state 2 is the correct boundary state. State 3 becomes the boundary state when the flow direction is reversed. Implementation of the finite wave model boundary conditions involves identifying states **a** and **b** in the discrete setting and describing how the flow solver makes use of the boundary state. This is covered in a later section.

Clearly, if a wave exiting a boundary is an acoustic or entropy wave, then the application of the finite wave boundary condition is exact, and any reflection can be no larger than the truncation error associated with the numerical scheme as it is applied to the convection of that wave. However, if an exiting wave is not an acoustic or convecting wave, it will nonetheless be approximated by one of these wave types at the boundary. The extent to which this approximation is in error will be the same extent to which a spurious reflection will occur. For example, a shock wave exiting the boundary would be modeled as an isentropic compression. It is well known[13] that the jump in entropy across a weak shock of strength $\Delta P$ is proportional to $(\Delta P)^3$. Therefore, the application of the finite wave model to such an outgoing shock wave would produce an $\mathcal{O}[(\Delta P)^3]$ spurious reflection.

## Multidimensional Extensions

As with all Riemann solvers, the choice of the wave structure used by the finite wave model represents a basis set, and the accuracy of the model depends only on the validity of that set. The limited choice in one dimension leaves little room for error. In multidimensions, however, the number of possible distinct waves becomes unlimited. If the identity and orientation of all waves were known, then a model could be formulated and solved for the boundary condition. Because this information is seldom known, several specific cases that are more manageable are considered instead.

The first, and simplest, multidimensional case is to assume that the same three waves exist as a coplanar structure but are not aligned with either the flow direction or the boundary. Under this assumption, the only new parameter introduced into the finite wave model is the wave angle. Figure 3 illustrates two flows for which this assumption is reasonable and for which the angle of the wave can be reasonably approximated. The first case (Fig. 3a) is a subsonic flow in which the noise-producing flow is well within the interior of the domain. The primary wave front is assumed to be circular with a center that is shifted downstream of the source due to convection. The second case (Fig. 3b) is a supersonic flow in which the component of the flow that is normal to the boundary is subsonic. In this case, the primary waves are aligned with the Mach lines. However, if the wave is strong or the boundary is far from the source, then an acoustic wave of this type will coalesce into a shock. In this event, neither the finite wave model (based on acoustic waves) nor the characteristic-based approach will be accurate.

The one-dimensional equations, Eqs. (1a–1f), are easily modified for these types of flows by applying them in the frame of reference of the wave. Thus,

$$V_2 - V_1 = -\frac{2n}{\gamma - 1}(a_2 - a_1)\,N \tag{3a}$$

$$\frac{a_2}{a_1} = \left(\frac{P_2}{P_1}\right)^{\frac{\gamma-1}{2\gamma}} \tag{3b}$$

$$N \cdot V_2 = N \cdot V_3 \tag{3c}$$

$$P_2 = P_3 \tag{3d}$$

$$V_4 - V_3 = +\frac{2n}{\gamma - 1}(a_4 - a_3)\,N \tag{3e}$$

$$\frac{a_4}{a_3} = \left(\frac{P_4}{P_3}\right)^{\frac{\gamma-1}{2\gamma}} \tag{3f}$$

where $V$ denotes the velocity vector and $N$ denotes a unit vector that is normal to the wave structure and points toward the interior of the domain. A careful count of the number of equations and unknowns reveals that the wave direction can be determined from the solution to Eqs. (3a–3f). In particular, $N=(V_1 - V_2)/\|V_1 - V_2\|$.

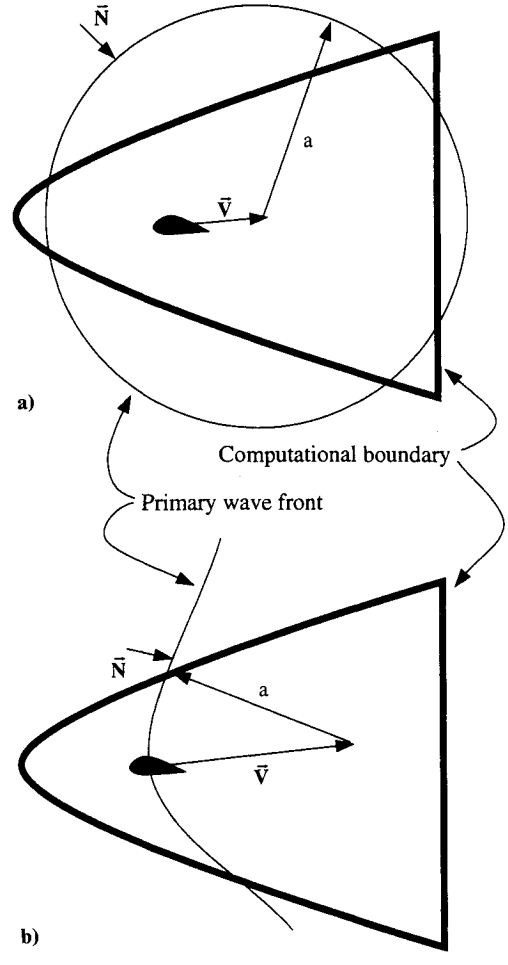


**Fig. 3 Two cases in which acoustic waves reaching the outer boundary have a predictable wave angle: a) subsonic freestream and b) supersonic freestream.**

In practice, however, this approach of predicting the wave angle from the local flow perturbations did not give acceptable results.

A modification to the one-dimensional finite wave model that does work well is to apply the model only to the component of the velocity that is normal to the wave front, $U_k \equiv \boldsymbol{N} \cdot \boldsymbol{V}_k$, for $k = 1, 2, 3$, and 4. In this approach, $\boldsymbol{N}$ is prescribed, and the multidimensional finite wave model becomes

$$\boldsymbol{N} \cdot (\boldsymbol{V}_2 - \boldsymbol{V}_1) = -\frac{2n}{\gamma - 1}(a_2 - a_1) \tag{4a}$$

$$\frac{a_2}{a_1} = \left(\frac{P_2}{P_1}\right)^{\frac{\gamma-1}{2\gamma}} \tag{4b}$$

$$\boldsymbol{N} \cdot \boldsymbol{V}_2 = \boldsymbol{N} \cdot \boldsymbol{V}_3 \tag{4c}$$

$$P_2 = P_3 \tag{4d}$$

$$\boldsymbol{N} \cdot (\boldsymbol{V}_4 - \boldsymbol{V}_3) = \frac{2n}{\gamma - 1}(a_4 - a_3) \tag{4e}$$

$$\frac{a_4}{a_3} = \left(\frac{P_4}{P_3}\right)^{\frac{\gamma-1}{2\gamma}} \tag{4f}$$

The components of the velocity that are tangent to the wave front are obtained by applying a local constraint on the vorticity. This is in contrast to the characteristic approach in which the boundary-tangent components of velocity $\boldsymbol{V}_t$ are obtained directly from either state **a** or state **b** depending on the flow direction. In the finite wave model, $\boldsymbol{V}_t$ on an inflow boundary is obtained by specifying the local vorticity to be zero. This approach allows fluctuations due to an oblique outgoing acoustic wave to be correctly modeled. At an outflow boundary, $\boldsymbol{V}_t$ is obtained from the interior, state **b**, just as in a characteristic approach.

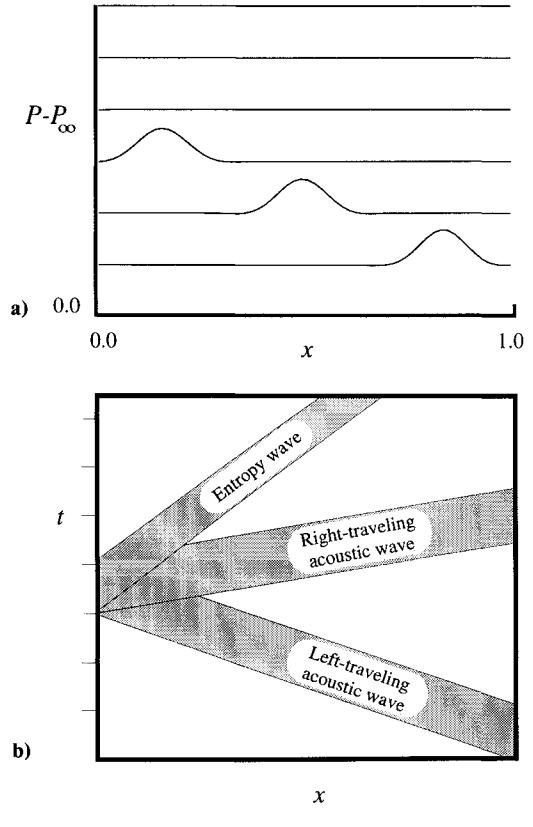


**Fig. 4 Schematic diagram of one-dimensional test problem showing a) propagation of a left-traveling acoustic pulse and b) paths of all possible waves.**

Next, a multidimensional extension that is appropriate for internal flows is considered. In aeroacoustical analysis of ducts, nozzles, and inlets, the sound source is often specified at an inflow or outflow boundary. For example, at an $x$ = constant boundary, the source may consist of pairs of oblique waves of the form

$$P(y, t) = P_\infty + \sum_m \tilde{P}_m \sin(\omega_m t)\cos(m\pi y/h) \tag{5}$$

where $\omega$ is the frequency, $m$ is the wave number in $y$, and $h$ is the channel half-height. If the mean flow in the channel is uniform, then each term in the series produces a pair of oblique waves of the form

$$P(x, y) = P_\infty + \sum_m {}^1\!/_2 \tilde{P}_m [\sin(\alpha x + \beta y + \omega t) + \sin(\alpha x - \beta y + \omega t)] \tag{6}$$

where $\alpha$ and $\beta$ depend on $\omega$, $m$, $h$, and the Mach number of the flow.

A single pair of oblique waves will be used as the basis for the second multidimensional extension to the finite wave model. Consider a pair of left-traveling acoustic waves of the form

$$P_1(x, y) \equiv P_\infty + {}^1\!/_2 \varepsilon \sin(\alpha x + \beta y) \tag{7a}$$

$$\frac{a_1}{a_\infty} = \left(\frac{P_1}{P_\infty}\right)^{\frac{\gamma-1}{2\gamma}} \tag{7b}$$

$$\boldsymbol{V}_1(x, y) - \boldsymbol{V}_\infty = -\frac{2}{\gamma - 1}(a_1 - a_\infty)\boldsymbol{N}^+ \tag{7c}$$

$$P_2(x, y) \equiv P_1(x, y) + {}^1\!/_2 \varepsilon \sin(\alpha x - \beta y) \tag{7d}$$

$$\frac{a_2}{a_1} = \left(\frac{P_2}{P_1}\right)^{\frac{\gamma-1}{2\gamma}} \tag{7e}$$

$$\boldsymbol{V}_2(x, y) - \boldsymbol{V}_1(x, y) = -\frac{2}{\gamma - 1}(a_2 - a_1)\boldsymbol{N}^- \tag{7f}$$

$$\boldsymbol{N}^\pm = \frac{(\alpha \hat{i} \pm B\hat{j})}{\sqrt{\alpha^2 + \beta^2}} \tag{7g}$$

Here, the subscripts refer to general states and do not correspond to the states indicated in Fig. 3. Solving for $\boldsymbol{V}_2$ gives

$$\boldsymbol{V}_2(x, y) - \boldsymbol{V}_\infty = \frac{2}{\gamma - 1}(a_1 - a_\infty)\boldsymbol{N}^+ - \frac{2}{\gamma - 1}(a_2 - a_1)\boldsymbol{N}^- \tag{8}$$

or

$$u_2 - u_\infty = \frac{-2\tilde{\alpha}}{\gamma - 1}(a_2 - a_\infty) \tag{9a}$$

$$v_2 - v_\infty = \frac{2\tilde{\beta}}{\gamma - 1}(2a_2 - a_1 - a_\infty) \tag{9b}$$

$$\tilde{\alpha} = \frac{\alpha}{\sqrt{\alpha^2 + \beta^2}} \tag{9c}$$

$$\tilde{\beta} = \frac{\beta}{\sqrt{\alpha^2 + \beta^2}} \tag{9d}$$

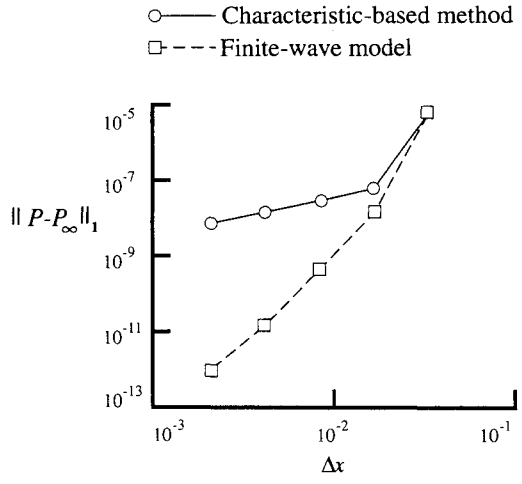


**Fig. 5 Pressure error at $t = 4.5\ t_p$.**

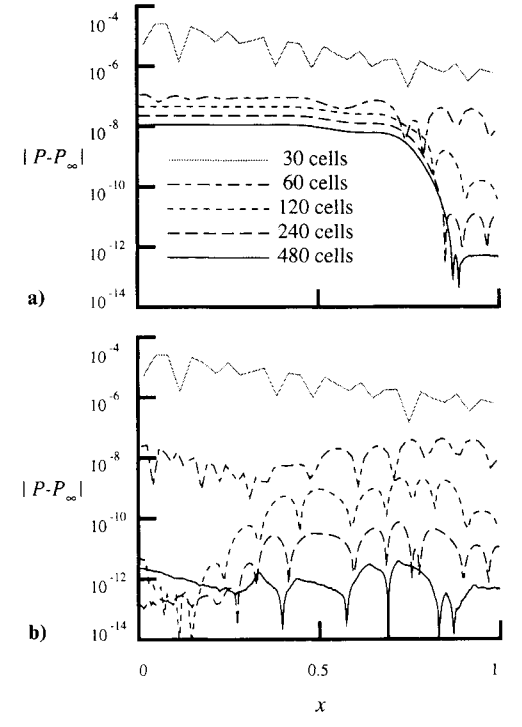


**Fig. 6 Pressure error at $t = 4.5\ t_p$ using a) characteristic-based boundary conditions and b) finite wave model.**

The $u$ component of velocity does not depend on the intermediate state, which implies that the one-dimensional finite wave model discussed earlier can be used to relate the total pressure fluctuation to the $u$ component when the scale factor $\tilde{\alpha}$ is taken into account. The $v$ component can be determined as described previously.

## Numerical Implementation

For this discussion, assume that the boundary condition can be written as a function $U_{bc} = F(U_a, U_b)$, where the function $F$ denotes the appropriate version of the finite wave model. The values $U_a$ are the prescribed ambient conditions. The values $U_b$ are determined from values that are interior to the domain in a manner that depends on the type of flow solver used: finite volume or finite difference. In the finite volume approach used here, point values of the solution on the cell face are computed from the cell average values using a procedure referred to as reconstruction. There are two values associated with each cell face, which correspond to the two sides of the face. The flux through the cell face is determined by application of a Riemann solver to the two face values. At the domain boundaries, cells are constructed such that the cell faces coincide with the boundaries. The face value on the interior side of the domain, which is taken as $U_b$, is readily determined by a reconstruction that is biased to the interior of the domain. The result of the boundary function $U_{bc}$ defines the face value that is on the exterior side. The Riemann solver can now be applied to the boundary cell face in the same way it is applied at an interior cell face. A minor simplification is to evaluate the boundary flux directly from $U_{bc}$ and eliminate the Riemann solver at the boundary.

Although all of the results presented in the next section were obtained with a finite volume method, the finite wave model has also been applied to a high-order accurate finite difference method. In the finite difference approach, the boundary function is used as a filter to modify the boundary values after the flow solver has been applied to all boundary and interior points. Thus, $U_b$ is defined as the boundary value after the solution has been advanced in time by the flow solver, and $U_{bc}$ is the value that replaces $U_b$ before the next time step is performed.

In the following section, the finite wave model is compared with a characteristic-based nonreflecting boundary condition, using a finite volume flow solver. Because most characteristic methods for nonreflecting boundary conditions that are found in the literature are formulated with a finite difference method in mind, a descrip-

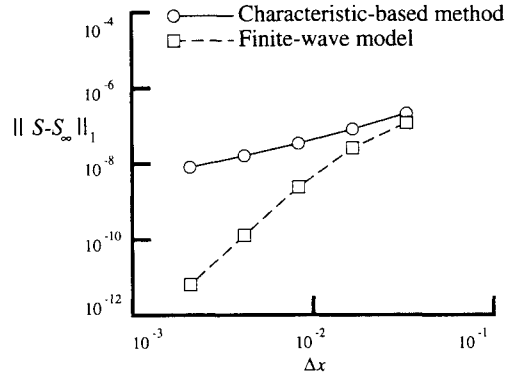


**Fig. 7 Entropy error at $t = 6.0\ t_p$.**

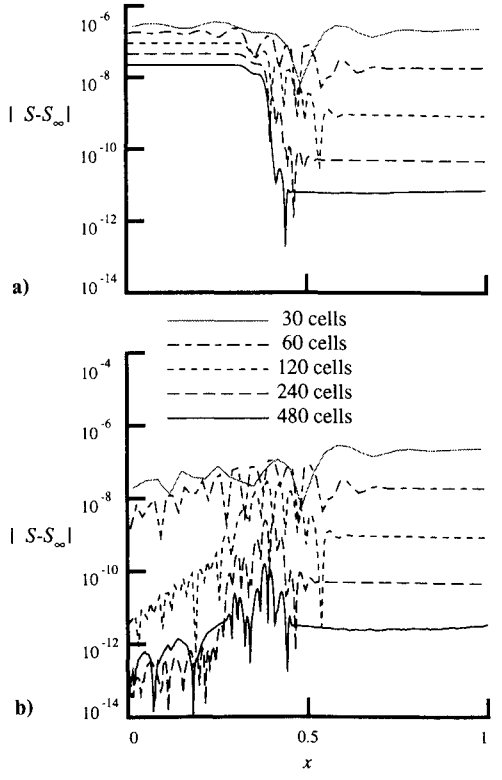


**Fig. 8 Entropy error at $t = 6.0\ t_p$ using a) characteristic-based boundary conditions and b) finite wave model.**

tion of the characteristic method used here is needed. Using the terminology of Hedstrom,[3] one can state the characteristic-based nonreflecting boundary condition as follows: the time derivatives of the characteristic variables associated with all inbound waves are zero. The remaining unknowns are determined by an extrapolation from the interior of those characteristic variables that are associated with outbound waves. In the finite volume approach, the time derivatives of the characteristic variables associated with inbound waves are zeroed, just as is done in the finite difference approach. For the outbound waves, however, the time derivatives of the associated characteristic variables are computed from the time derivative of the boundary values reconstructed from interior cell averages.

## Numerical Validation

The initial validations are performed for a one-dimensional channel flow in which a single left-traveling acoustic pulse is applied at the outflow boundary. When the initial pulse reaches the upstream boundary at $t = t_1$, it should exit the domain and leave a uniform flow, as illustrated in Fig. 4a. In practice, most boundary conditions will produce reflections that consist of a right-traveling acoustic wave and a convecting entropy wave. In the present test case, these reflections are weak and are not visible when viewed on the scale of the initial pulse; however, the paths they should follow are illustrated in Fig. 4b. Shortly after $t_1$, the solution is dominated by the faster moving acoustic wave. At a much later time, the reflected acoustic wave has left the domain, which leaves only the convective wave. The error due to the right-traveling acoustic wave is measured by comparing the point-wise pressure to the expected constant value; the error attributed to the convective wave is measured by comparing the entropy (specifically, the quantity $S \equiv P/\rho^{\gamma}$) to its correct value. The problem has been scaled such that $t_1 = 3\ t_p$, where $t_p$ is the time required for the pulse

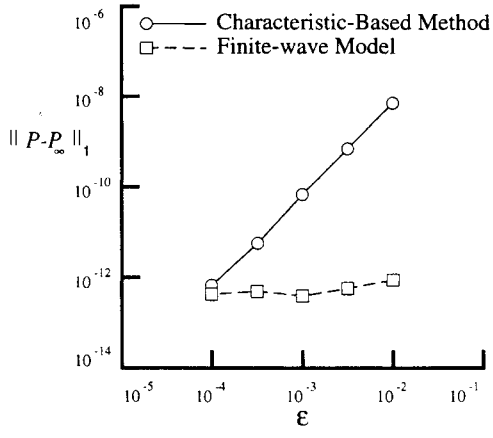


**Fig. 9 Influence of wave amplitude on pressure error at $t = 4.5\ t_p$.**

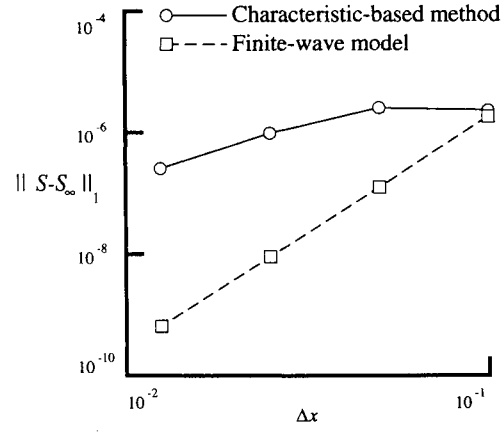


**Fig. 10 Entropy error at $t = 9.0\ t_p$ for a nonplanar source in a two-dimensional channel.**

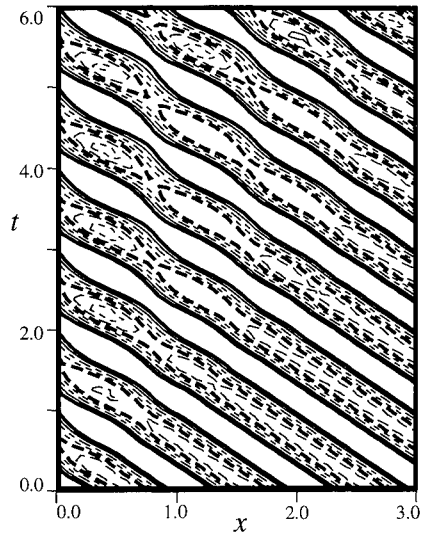


**Fig. 11 Contours of centerline pressure for a nonplanar source in a two-dimensional channel with characteristic-based boundary conditions applied at the left boundary.**

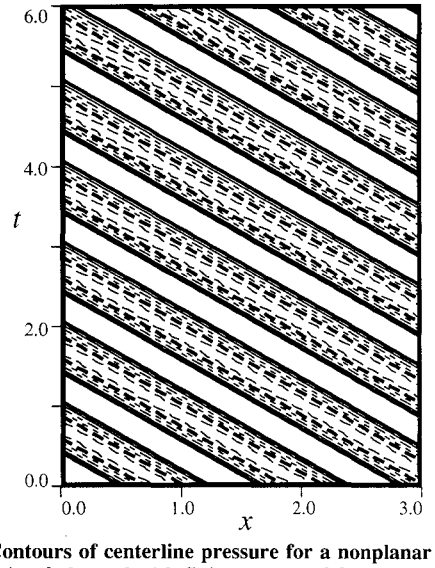


**Fig. 12 Contours of centerline pressure for a nonplanar source in a two-dimensional channel with finite wave model boundary conditions applied at the left boundary.**

to enter the domain. The flow is initially uniform with a Mach number of 0.3, and the pulse is of the form

$$P_{\text{exit}}(t) = \begin{cases} P_\infty [1 + \varepsilon \sin^4(\pi t/t_p)], & 0 \le t < t_p \\ P_\infty, & t \ge t_p \end{cases} \tag{10}$$

Figure 5 shows the $L_1$ norms of the pressure error as a function of mesh size for a wave amplitude $\epsilon = 0.01$ and $t = 4.5\ t_p$. Results are shown for both the finite wave model and the characteristic approach; in both cases, the numerical flow solver used in the interior is a fourth-order ENO method. The finite wave model preserves the high-order convergence of the flow solver, but the characteristic method shows first-order convergence. An examination of the solutions at $t = 4.5\ t_p$, shown in Figs. 6a and 6b, reveals that both methods produce reflections, as expected, and further confirms that the reflections produced by the finite wave model are of high order. This suggests that the reflections produced by the finite wave model are due to the truncation error of the numerical solver used in the interior.

Similar results are presented in Figs. 7 and 8, in which the $L_1$ norms of the entropy error are given at $t = 6.0\ t_p$. As before, both methods produce an erroneous convective wave that behaves first

order for the characteristic method but high order for the finite wave model.

Figure 9 shows the pressure error at $t = 4.5\ t_p$ for both boundary treatments as a function of wave amplitude, for a case in which the grid is fixed with 480 cells. As expected, the error for the finite wave model is on the same order for all tested wave amplitudes. However, the error in the characteristic-based treatment is proportional to the square of the wave amplitude, or $E(\epsilon) \propto \epsilon^2$. This is consistent with the first-order behavior observed in the grid refinement study and suggests that the error is associated with the linearization that is inherent in the characteristic approach. The relation between the grid-refinement and the $\epsilon$-refinement errors can be explained as follows. If the error is assumed to accumulate linearly in time, the $\epsilon$ refinement implies that the error produced during each time step is also proportional to the amplitude: $E_{\Delta t} = E(\epsilon)/N \propto \epsilon^2/N \propto \epsilon^2$ (recall that the number of time steps $N$ is fixed during the $\epsilon$ refinement). The observation that locally the only effect of changing the wave amplitude is to change the local variation of the solution $U^{n+1} - U^n \equiv \delta U \propto \epsilon$ implies that $E_{\Delta t} \propto (\delta U)^2$. The grid-refinement study gives $E(\Delta x) \propto \Delta x$, which implies $E_{\Delta t} = E(\Delta x)/N \propto \Delta x/N \propto (\Delta x)^2$. As the grid is refined, the variation of the solution over a single time step decreases in direct proportion to the mesh size, which implies $E_{\Delta t} \propto (\delta U)^2$, just as in the $\epsilon$-refinement study.

Next, a two-dimensional channel flow is considered in which a single pair of oblique waves is prescribed at the outflow boundary. As in the one-dimensional case, the initial flow is uniform with a Mach number of 0.3; however, the presence of the top and bottom walls prohibits the use of the pulsed excitation. The form of the exit pressure is given by Eq. (5) for $m = 1$. The frequency was chosen such that the waves are inclined at 45 deg; thus, $\tilde{\alpha} = \tilde{\beta} = \sqrt{2}/2$. The finite wave model is applied at the inflow boundary by using the exact value of $\alpha$. The $v$ component of velocity is determined by forcing the flow to remain irrotational. Because the exit conditions are excited continuously, the pressure is never uniform, and a reflected acoustic wave is not easily detected. Consequently, the validation of this case is limited to checking for the presence of entropy waves. Figure 10 shows the $L_1$ norm of the entropy error at $t = 9\ t_p$ for both the finite wave model and the characteristic boundary conditions. Just as in the one-dimensional case, the finite wave model gives high-order convergence. However, the characteristic method gives second-order convergence. Although the characteristic method, in two dimensions, is usually written in terms of $v$ directly, a case with $v$ determined from a vorticity relation showed no improvement. Although it is difficult to obtain a quantitative measure of the reflected acoustic waves, Figs. 11 and 12, which show contours of the centerline pressure, provide a qualitative indication. In Fig. 11, which shows the results of the characteristic-based boundary conditions, there is a clear distortion of the prescribed left-traveling wave that is not present in Fig. 12, when the finite wave boundary condition is used.

## Conclusions

The finite wave model has been presented and compared with characteristic-based, nonreflective boundary conditions for acoustic flowfields, which are simulated by a fourth-order numerical flow solver. The characteristic approach is accurate for extremely weak waves but reduces the accuracy to first order in mesh size when wave amplitudes are nontrivial. The finite wave model preserves the high-order convergence of the flow solver independent of wave amplitude, and works equally well in multidimensions if the wave angle is known or can be closely approximated.

## Acknowledgment

The work of the second author was supported by the U.S. Government under Contract NAS1-19672.

## References

[1]Streett, C. L., and Macaraeg, M. G., "Spectral Multi-Domain for Large-Scale Fluid Dynamic Simulations," *Applied Numerical Mathematics,* Vol. 6, Dec. 1989, pp. 123–139.

[2]Liu, Z., and Liu, C., "Fourth-Order Finite Difference and Multigrid Methods for Modeling Instabilities in Flat Plate Boundary Layers," *Journal of Wind Engineering,* Vol. 52, Aug. 1992, pp. 412–417.

[3]Hedstrom, G. W., "Nonreflecting Boundary Conditions for Nonlinear Hyperbolic Systems," *Journal of Computational Physics,* Vol. 30, No. 2, 1979, pp. 222–237.

[4]Thompson, K. W., "Time Dependent Boundary Conditions for Hyperbolic Systems," *Journal of Computational Physics,* Vol. 68, No. 1, 1987, pp. 1–24.

[5]Engquist, B., and Majda, A., "Absorbing Boundary Conditions for the Numerical Simulation of Waves," *Mathematics of Computation,* Vol. 31, July 1977, pp. 629–651.

[6]Roe, P. L., "Upwind Schemes Using Various Formulations of the Euler Equations," *Proceedings of the INRIA Workshop on Numerical Methods for the Euler Equations of Fluid Dynamics* (France), SIAM, Philadelphia, PA, 1983, pp. 14–31.

[7]Giles, M. B., "Non-Reflecting Boundary Conditions for Euler Equation Calculations," AIAA Paper 89-1942, June 1989.

[8]Saxer, A. P., and Giles, M. B., "Quasi-3-D Non-Reflecting Boundary Conditions for Euler Equation Calculations," AIAA Paper 91-1603, June 1991.

[9]Richtmyer, R. D., and Morton, K.W., *Difference Methods for Initial-Value Problems,* Wiley, New York, 1967.

[10]Casper, J., and Atkins, H. L., "A Finite-Volume High-Order ENO Scheme for Two-Dimensional Hyperbolic Systems," *Journal of Computational Physics,* Vol. 106, May 1993, pp. 62–76.

[11]Atkins, H. L., "High-Order ENO Methods for the Unsteady Compressible Navier-Stokes Equations," AIAA Paper 91-1557, June 1991.

[12]Osher, S., and Chakravarthy, S., "Upwind Schemes and Boundary Conditions with Applications to Euler Equations in General Geometries," *Journal of Computational Physics,* Vol. 50, No. 3, 1983, pp. 447–481.

[13]Liepmann, H. W., and Roshko, A., *Elements of Gasdynamics,* Wiley, New York, 1957.